Developmental Biology 330 (2009) 250–262

Contents lists available at ScienceDirect

Developmental Biology

journal homepage: www.elsevier.com/developmentalbiology

Drosophila Atlastin regulates the stability of muscle microtubules and is required for synapse development

Mihye Lee [a,b], Sang Kyoo Paik [c], Min-Jung Lee [a], Yoon-Jung Kim [a], Sungdae Kim [a], Minyeop Nahm [a], Soo-Jin Oh [a,d], Hyun-Man Kim [a], Jeongbin Yim [b], C. Justin Lee [d], Yong Chul Bae [c], Seungbok Lee [a,*]

[a] Department of Cell and Developmental Biology, Dental Research Institute, School of Dentistry, Seoul National University, Seoul 110-740, Republic of Korea
[b] School of Biological Sciences, Seoul National University, Seoul 110-740, Republic of Korea
[c] Department of Oral Anatomy and Neurobiology, School of Dentistry, Kyungpook National University, Daegu 700-412, Republic of Korea
[d] Center for Neural Science, Korea Institute of Science and Technology, Seoul 136-791, Republic of Korea

ARTICLE INFO

Article history:
Received for publication 24 October 2008
Revised 18 March 2009
Accepted 22 March 2009
Available online 31 March 2009

Keywords:
Drosophila
Atl
Spastin
Synaptic growth
Neuromuscular junction
ER and Golgi morphogenesis
Microtubule stability
Hereditary spastic paraplegia

ABSTRACT

Hereditary spastic paraplegia (HSP) is an inherited neurological disorder characterized by progressive spasticity and weakness of the lower extremities. The most common early-onset form of HSP is caused by mutations in the human gene that encodes the dynamin-family GTPase Atlastin-1 (Atl-1). Recently, loss of the *Drosophila* ortholog of Atl-1 (Atl) has been found to induce locomotor impairments from the earliest adult stages, suggesting the developmental role of atlastin-subfamily GTPases. Here, we provide evidence that Atl is required for normal growth of muscles and synapses at the neuromuscular junction (NMJ). Atl protein is highly expressed in larval body-wall muscles. Loss-of-function mutations in the *atl* gene reduce the size of muscles and increase the number of synaptic boutons. Rescue of these defects is accomplished by muscular, but not neuronal expression of Atl. Loss of Atl also disrupts ER and Golgi morphogenesis in muscles and reduces the synaptic levels of the scaffold proteins Dlg and α-spectrin. We also provide evidence that Atl functions with the microtubule-severing protein Spastin to disassemble microtubules in muscles. Finally, we demonstrate that the microtubule-destabilizing drug vinblastine alleviates synapse and muscle defects in *atl* mutants. Together, our results suggest that Atl controls synapse development and ER and Golgi morphogenesis by regulating microtubule stability.

© 2009 Elsevier Inc. All rights reserved.

Introduction

The hereditary spastic paraplegias (HSPs) are a group of inherited neurological disorders characterized primarily by progressive spasticity and weakness of the lower extremities (Fink, 2003; Reid, 2003; Soderblom and Blackstone, 2006). Spastic paraplegia occurs in isolation in pure HSPs, and is accompanied by additional neurological symptoms in complicated HSPs (Harding, 1983). These disorders are caused by developmental defects or retrograde degeneration of the long corticospinal tract axons (Reid, 2003). To date, more than 25 different chromosomal loci have been mapped for HSPs with autosomal dominant, autosomal recessive, or X-linked pattern of inheritance, and 11 associated genes have been molecularly identified (Soderblom and Blackstone, 2006). Mutations in *atlastin-1* (*atl-1*, *SPG3A*) and *spastin* (*SPG4*) have been estimated to cause approximately 10% and 40% of autosomal dominant pure HSP, respectively (Reid, 2003).

The *atl-1* gene encodes a protein that consists of an N-terminal GTPase domain with three conserved GTP-binding motifs and two C-terminal transmembrane (TM) domains (Praefcke and McMahon, 2004; Zhao et al., 2001). The GTPase domain of the Atl-1 protein shows high sequence similarity to those found in the dynamin-family large GTPases. In humans, there are two additional members of the atlastin subfamily: Atl-2 and Atl-3 (Zhu et al., 2003). Biochemical studies have shown that all atlastin-subfamily members are integral membrane proteins and capable of forming homo-oligomers in vivo (Rismanchi et al., 2008; Zhu et al., 2003). The Atl-1 protein is expressed at high levels in the central nervous system (CNS) but is also detected at lower levels in other nonneural tissues (Zhu et al., 2003). In contrast, high expression of Atl-2 and Atl-3 is observed in nonneural tissues (Rismanchi et al., 2008). At the subcellular level, Atl-1 is predominantly localized to the *cis*-Golgi apparatus and, to a lesser extent, the endoplasmic reticulum (ER) (Namekawa et al., 2007; Zhu et al., 2003, 2006), while Atl-2 and Atl-3 are largely located in the ER and vesicular tubular complexes (VTCs) (Rismanchi et al., 2008). Consistent with their subcellular localization, atlastin proteins have been implicated in ER and Golgi morphogenesis. Expression of dominant-negative forms of Atl-1, Atl-2, or Atl-3 disrupts the morphology of the ER and Golgi apparatus in heterologous cell culture systems (Namekawa et al., 2007; Rismanchi et al., 2008).

* Corresponding author.
E-mail address: seunglee@snu.ac.kr (S. Lee).

0012-1606/$ – see front matter © 2009 Elsevier Inc. All rights reserved.
doi:10.1016/j.ydbio.2009.03.019

Atl-1 is also required for axonal growth during neuronal development. In primary cultures of developing cortical neurons, Atl-1 is enriched in axonal growth cones, and RNAi-mediated *atl-1* knockdown impairs neurite formation and outgrowth (Zhu et al., 2006). Together with the key characteristic feature of *atl-1* mutations – the very early-onset of symptoms (Namekawa et al., 2006) – these findings support the hypothesis that developmental failure may represent an etiology of the SPG3A form of HSP. However, in vivo evidence to support the developmental function of Atl-1 has yet to be reported.

What is the molecular mechanism by which Atl-1 regulates ER and Golgi morphology and axon elongation? An important clue to this open question has come from two recent studies demonstrating that Atl-1 physically interacts with Spastin, another HSP protein that is a microtubule-severing AAA ATPase (ATPase associated with various cellular activities) (Evans et al., 2006; Sanderson et al., 2006). Consistently, *spastin* mutations have been shown to disrupt microtubule-based distribution of membranous organelles and axonal outgrowth (McDermott et al., 2003; Wood et al., 2006). Thus, it is tempting to speculate that Atl-1 plays an essential role in various cellular and developmental events by regulating microtubule networks. However, the involvement of Atl-1 in Spastin-dependent microtubule disassembly has yet to be demonstrated.

We have previously shown that a single ortholog of mammalian atlastins exists in *Drosophila* (Lee et al., 2008). In the present study, we investigated its cellular and developmental functions in the neuromuscular system. We show that this protein is highly expressed in the larval body-wall muscles. Loss of Atl leads to abnormal growth of the muscle and neuromuscular junction (NMJ) synapse as well as defects in ER and Golgi morphogenesis, and these phenotypes are rescued by muscle-specific expression of Atl. We also provide genetic evidence that Atl acts through Spastin to regulate microtubule stability. Finally, our pharmacological experiments indicate that microtubule misregulation accounts for developmental defects induced by *atl* mutations. These results reveal a novel role for Atl in Spastin-dependent microtubule disassembly and synapse development.

Results

Generation of an atl null mutant

To directly test the developmental role of Atl, we generated deletion mutants by imprecise excision of atl^1, a viable P-element insertion in the first intron of the *Drosophila atl* gene (Lee et al., 2008), and determined the breakpoints of mutants by PCR and sequence analysis. Among the mutants, atl^2 had an approximately 1.6 kb deletion within the *atl* locus that removed the DNA encoding exon 3 through exon 4 (Fig. 1A). The deleted exons are common to two predicted alternative transcripts of *atl*.

The *atl* gene is essential, since mutants bearing the atl^2 allele as a homozygote or in a heteroallelic combination with the deficiency *Df (3R)Exel7357* (referred to hereafter as *Df*) that deletes the *atl* locus survive only to pupal stages with few adult escapers (~8%). The escapers have smaller body sizes compared to w^{1118} wild-type control flies and are sterile. Reverse transcription (RT)-PCR analysis revealed that expression of *atl* mRNA is abolished in atl^2/Df mutant larvae, while mRNA of the adjacent gene, *CG31127*, is normally expressed in the same larvae (Fig. 1B). Thus, atl^2 is null only for the *atl* gene.

Expression of Atl protein in the larval neuromusculature

To characterize the Atl protein, we generated a polyclonal antibody against an N-terminal region (amino acids 1–421) of the fly Atl protein. On western blots containing wild-type larval extracts, this antibody recognized a band of ~55 kDa that corresponds to the predicted size for Atl. The recognized protein was not detected in the larval extracts of atl^2 and atl^2/Df mutants (Fig. 1C), confirming the specificity of this anti-Atl antibody.

We then examined Atl expression in the nervous system of third instar larvae by immunohistochemical analysis using anti-Atl. In the larval CNS, Atl immunoreactivity was detected within neuropil regions of the brain and ventral nerve cord (VNC) (Fig. 1D). It was also detected motor axon bundles emanating from ventral ganglia at a lower level (Fig. 1D, arrow). However, Atl immunoreactivity was absent in the CNS of atl^2/Df mutant larvae (Fig. 1E), confirming the specificity of the Atl staining. In the neuromusculature, Atl signal was highly detected in the cytoplasm of body-wall muscles and weakly observed in proximal parts of presynaptic arbors (Figs. 1F, F′). However, it was not present within synaptic boutons at detectable levels (see Fig. 1H). The immunoreactivity was eliminated in both muscles and motor axons of atl^2/Df mutant larvae (Fig. 1G). To inspect Atl localization in the postsynaptic region of NMJ synapses, we analyzed larvae expressing the postsynaptic marker CD8-GFP-Shaker fusion protein under the control of the myosin heavy chain (MHC) promoter (Zito et al., 1999). Double labeling with an antibody against GFP revealed that Atl immunoreactivity does not extend into the postsynaptic area (Fig. 1H). In the muscle, Atl was detected primarily in a punctate pattern throughout the cytoplasm.

Atl functions in the postsynaptic muscle to control synaptic growth

Given the expression of Atl in the larval neuromusculature, we investigated whether it plays an essential role in synaptic morphogenesis at the NMJ. We first confirmed that pathfinding of motor axons was normal in atl^2/atl^2 and atl^2/Df embryos stained with mAb 1D4 (data not shown). We then compared NMJ morphology in wild-type (w^{1118}) and *atl* mutant larvae at the crawling third instar stage. Although we found no gross defects in the overall pattern of presynaptic terminals in *atl* mutants, we did observe a mild defect in synaptic growth. In wild-type larvae, type Ib boutons were linearly arranged along NMJ branches (Figs. 2A, A′). However, in atl^2/Df mutant larvae, Ib boutons were more clustered at the terminal regions of NMJ branches (Figs. 2B, B′). Some of them were small satellite boutons that are budding off from a large parental bouton (Torroja et al., 1999) (Fig. 2B′, arrows). To compare synaptic growth between wild-type and atl^2/Df mutant larvae, we counted bouton numbers at NMJ 6/7 in abdominal segment 2 (A2). Average bouton number per NMJ 6/7 was increased in atl^2/Df larvae compared with wild-type in a temperature-sensitive manner. Bouton number was ~17% higher at 25 °C (wild-type: 119.6 ± 3.0, $n = 31$; atl^2/Df: 139.5 ± 4.6, $n = 36$; $p < 0.001$) and ~42% higher at 18 °C (wild-type: 114.1 ± 3.7, $n = 20$; atl^2/Df: 162.2 ± 3.9, $n = 20$; $p < 0.0001$). Despite the change in the total number of boutons per NMJ 6/7, *atl* mutant larvae showed no significant difference in the proportion of Ib and Is boutons compared with wild-type larvae. We also observed a significant change in the size of body-wall muscle cells in atl^2/Df (Fig. 2E). The combined surface area of muscles 6 and 7 of segment A2 was reduced by ~31% in atl^2/Df larvae at 25 °C (wild-type: $88.5 \pm 1.2 \times 10^3$ μm^2; atl^2/Df: $61.2 \pm 0.9 \times 10^3$ μm^2; $p < 0.0001$) (Supplementary Fig. S1). This phenotype was also temperature-sensitive, with a reduction of the muscle surface area by ~17% at 18 °C (wild-type: $87.2 \pm 1.5 \times 10^3$ μm^2; atl^2/Df: $72.5 \pm 1.5 \times 10^3$ μm^2; $p < 0.0001$). When normalized to muscle surface area, bouton number was increased by ~70% in atl^2/Df at either 25 °C (wild-type: $1.36 \pm 0.03 \times 10^{-3}$ μm^{-2}; atl^2/Df: $2.28 \pm 0.07 \times 10^{-3}$ μm^{-2}; $p < 0.0001$) or 18 °C (wild-type: $1.31 \pm 0.03 \times 10^{-3}$ μm^{-2}; atl^2/Df: $2.24 \pm 0.05 \times 10^{-3}$ μm^{-2}; $p < 0.0001$) (Fig. 2F). At 25 °C, larvae homozygous for atl^2 also exhibited synaptic and muscle defects that were almost identical with those in atl^2/Df larvae (Fig. 2F, data not shown). The 13 kb genomic DNA fragment (*atl-Ge*) containing the *atl* gene (Lee et al., 2008) completely rescued the normalized numbers of boutons in atl^2/atl^2 larvae (Fig. 2F), suggesting that *atl*

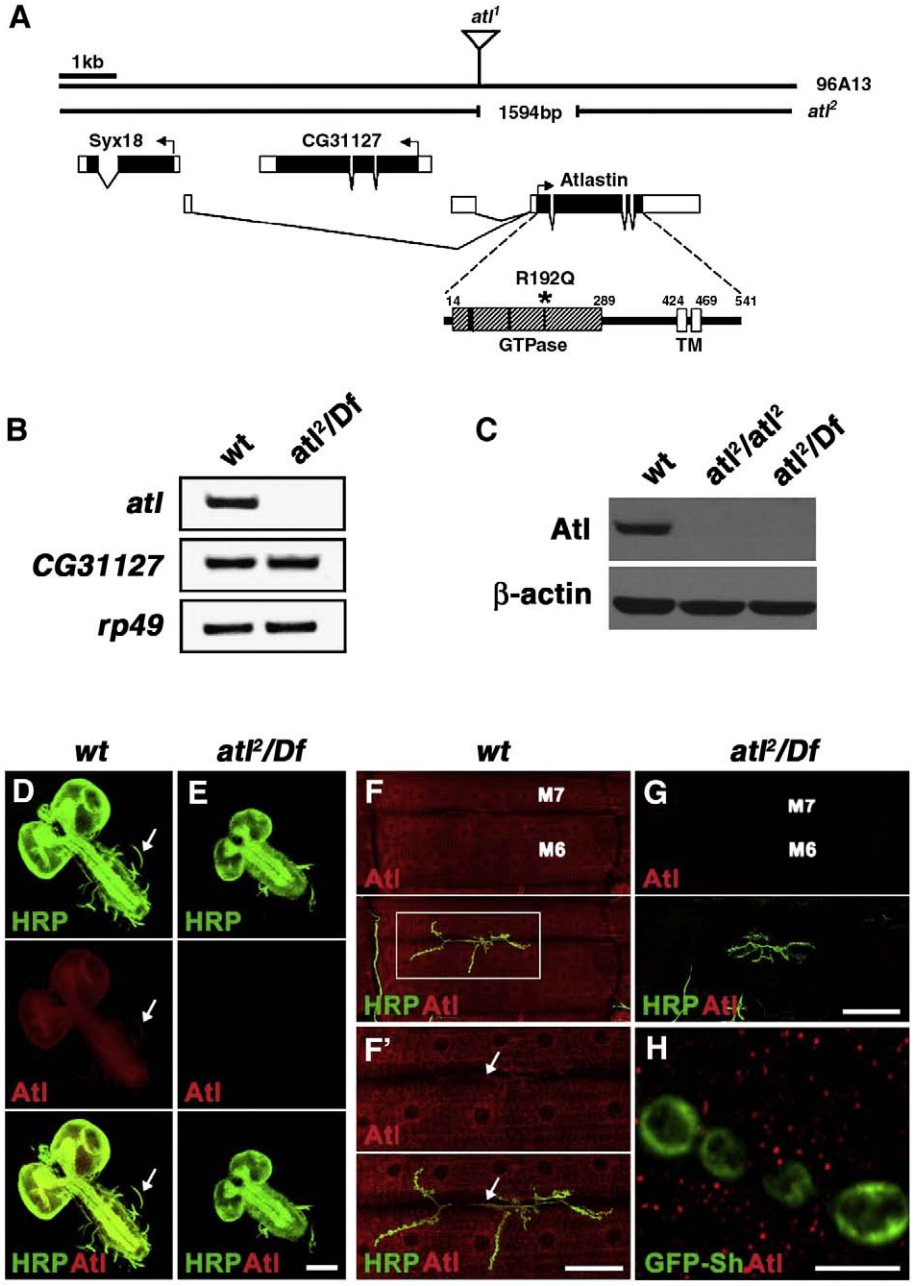

Fig. 1. Generation of *atl* null mutant and expression of Atl protein in the larval neuromusculature. (A) Genomic structure of the *atl* locus and mapping of an *atl* null mutant. The inverted triangle marks the insertion site of a P-element line atl^1. The extent of the deletion in atl^2 generated by imprecise excision of atl^1 is indicated by the broken line. Below are the exon/intron structures of the transcripts for *atl* and its neighboring genes, *CG31127* and *Syx18*. Exons are indicated by boxes, coding regions by black boxes, and translation start sites by bent arrows. *atl* is predicted to generate two alternative transcripts, both of which have the same open reading frame (ORF). The domain structure of the Atl protein is also shown at the bottom. The asterisk denotes a dominant-negative mutation of Atl (Atl^{R192Q}) used in this study. GTPase, a GTPase domain (cross-hatched box) with tripartite GTP-binding motifs (black lines); TM, two transmembrane domains (white boxes). Scale bar: 1 kb. (B) RT-PCR analysis of wild-type (*wt*) and $atl^2/Df(3R)Exel7357$ (atl^2/Df) third instar larvae. Note that *atl* mRNA expression was eliminated in atl^2/Df larvae, while levels of *CG31127* and *rp49* mRNAs were not different between wild-type and atl^2/Df larvae. (C) Western blot analysis of body-wall muscles of wild-type, atl^2/atl^2, and atl^2/Df third instar larvae with anti-Atl antibody. The same blot was reprobed for β-actin as a loading control. (D, E) Confocal images of third instar larval brains of wild-type (D) and atl^2/Df (E) stained with anti-Atl (red) and anti-HRP (green), a neuronal membrane-specific marker (Jan and Jan, 1982). Note the low expression of Atl in axon bundles emerging from the ventral nerve cord (arrow). (F, G) Confocal images of third instar NMJs formed on muscles 6 and 7 (M6; M7) stained with anti-HRP (green) and anti-Atl (red) antibodies are shown for wild-type (F) and atl^2/Df (G). (F′) Higher magnification images of the area indicated by the box in F. Atl protein is highly expressed throughout the cytoplasm of wild-type body-wall muscles and also detected at lower levels in proximal parts of presynaptic arbors (arrow). Note that anti-Atl immunoreactivity is eliminated in atl^2/Df mutant muscles and presynaptic arbors. Anterior is to the left. (H) High magnification images of a third instar NMJ 6/7 stained with anti-Atl and anti-GFP antibodies. Animals were genetically manipulated to express the postsynaptic marker CD8-GFP-Shaker fusion protein in the muscle. Note the absence of Atl staining in the peribouton area labeled with CD8-GFP-Shaker. Scale bars: (D, E) 100 μm; (F, G) 100 μm; (F′) 50 μm; (H) 5 μm.

loss-of-function accounts for the observed defects in synapse and muscle growth.

To determine whether *atl* is required in the muscle or in the neuron for the regulation of synapse and muscle growth, we performed rescue experiments by expressing an *atl* cDNA (*UAS-atl*) under the control of tissue-specific GAL4 drivers in atl^2/Df animals. In the wild-type background, overexpression of *UAS-atl* using a muscle-specific *BG57-GAL4* driver at 25 °C, but not 18 °C, often led to abnormalities in muscle morphology (see below). We thus performed rescue experiments at 18 °C. In atl^2/Df mutant larvae bearing both

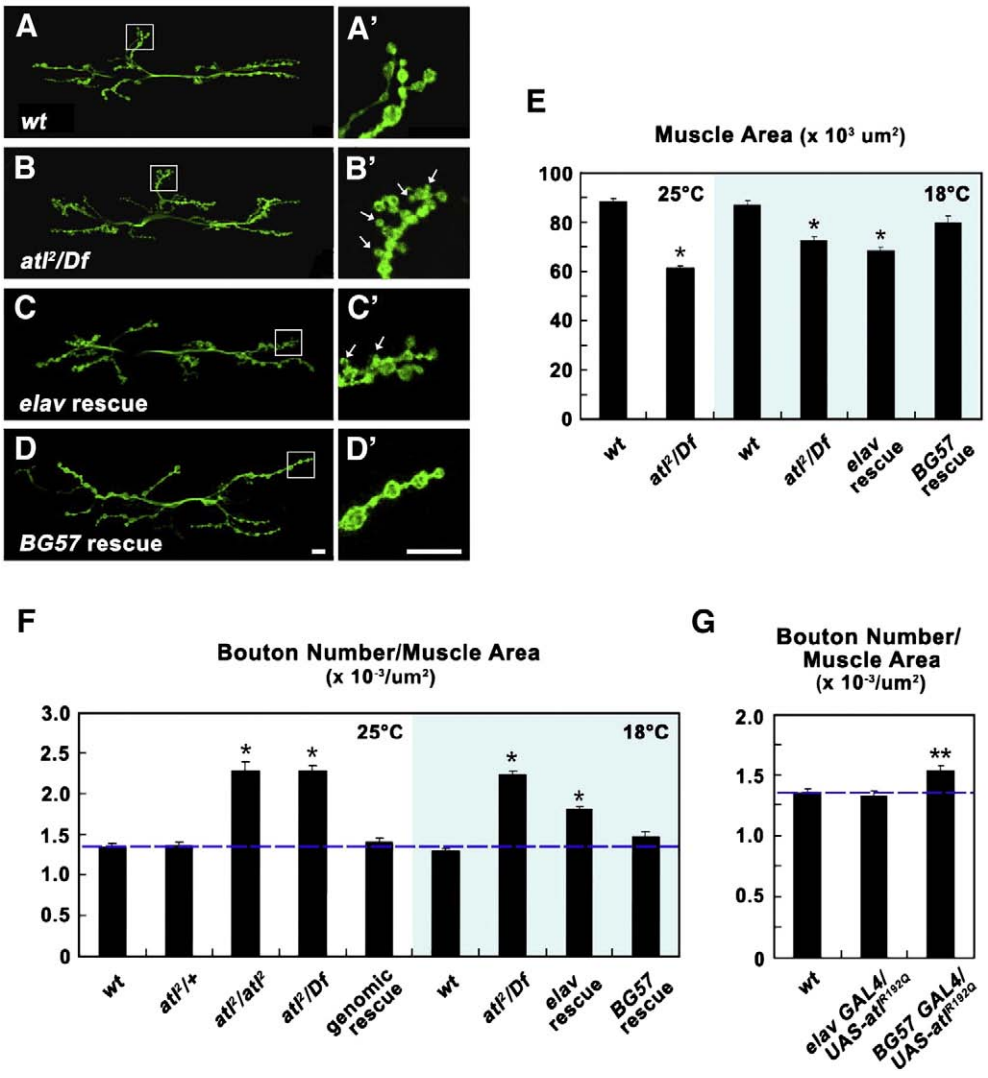

Fig. 2. Mutations in *atl* lead to an increase in synaptic bouton number and a decrease in muscle size. (A–D) Confocal images of NMJs on muscles 6 and 7 stained with anti-HRP antibody in wild-type (A), atl^2/Df (B), *elav-GAL4,atl²/UAS-atl,Df* (*elav* rescue, [C]), and *BG57-GAL4,atl²/UAS-atl,Df* (*BG57* rescue, [D]) third instar larvae raised at 18 °C. (A, B) Synaptic boutons are linearly arranged with regular intervals in wild-type, whereas they are densely clustered in atl^2/Df mutant NMJs due to increased satellite bouton formation. (C, D) Postsynaptic expression, but not presynaptic expression of *UAS-atl*, rescues the phenotype of increased satellite bouton formation. (A′–D′) Higher magnification views of the areas boxed in A–D. Arrows indicate satellite boutons. Scale bars: 10 μm. (E, F) Quantification of muscle 6/7 surface area (E) and presynaptic bouton number at NMJ 6/7 (F) in different genotypes raised at 25 °C or 18 °C. In (F), bouton numbers are normalized by the total surface area of muscles 6 and 7. The genotypes analyzed include wild-type (25 °C, $n=31$; 18 °C, $n=20$), $atl^2/+$ ($n=17$), atl^2/atl^2 ($n=13$), atl^2/Df (25 °C, $n=36$; 18 °C, $n=20$), *atl-Ge,atl²/atl-Ge,atl²* ([genomic rescue], $n=22$), *elav-GAL4,atl²/UAS-atl,Df* ([*elav* rescue], $n=17$), and *BG57-GAL4,atl²/UAS-atl,Df* ([*BG57* rescue], $n=14$). Data are mean ± SEM. Significant differences, as determined by Student's *t*-test, are denoted by an asterisk (control, wild-type; $p<0.0001$). (G) Quantification of bouton number at NMJ 6/7 in wild-type ($n=13$), *elav-GAL4/UAS-atl*^{R192Q} ($n=17$), and *BG57-GAL4/UAS-atl*^{R192Q} ($n=24$) larvae. Bouton numbers are normalized to the total surface area of muscles 6 and 7. Muscular but not neuronal expression of a dominant-negative form of Atl (Atl^{R192Q}) increases normalized bouton number. Data are mean ± SEM. A double asterisk indicates significant difference compared to the wild-type control ($p<0.007$).

UAS-atl and *BG57-GAL4*, the combined surface area of muscles 6 and 7 was partially restored (mean surface area of muscles 6 and 7 combined was $80.1 \pm 2.7 \times 10^3$ μm^2) (Fig. 2E). In addition, the bouton number normalized to muscle area was completely rescued to wild-type (Fig. 2F), and dense clusters of boutons were rarely observed (Figs. 2D, D′). In contrast, neuronal expression of *UAS-atl* using the *elav-GAL4* driver was not effective in rescuing either bouton number or muscle size (Figs. 2C, C′, E, F). In control experiments, we found that *elav-GAL* or *BG57-GAL4* alone did not affect synaptic and muscle growth (data not shown). Therefore, our data suggest that defects in synapse and muscle growth result from the loss of Atl primarily in the postsynaptic muscle.

We further investigated the role of Atl in synaptic growth by overexpressing its dominant-negative form with the UAS/GAL4 system (Brand and Perrimon, 1993). We have previously shown that the Atl^{R192Q} protein exerts a dominant-negative effect on wild-type Atl to produce *atl*-like phenotypes in adult flies (Lee et al., 2008). When Atl^{R192Q} was overexpressed specifically in neurons, the normalized bouton number at NMJ 6/7 was not changed (Fig. 2G). However, its overexpression in muscles led to a 13% increase in bouton number per muscle surface area (mean value was $1.53 \pm 0.04 \times 10^{-3}$ μm^{-2} in larvae expressing *UAS-atl*^{R192Q}; $p<0.007$) (Fig. 2G). These results support the idea that Atl primarily functions in postsynaptic muscle cells, rather than in motor neurons, to control synaptic growth.

Atl is required for normal expansion and organization of the subsynaptic reticulum

To determine if Atl is required for normal synaptic assembly, we analyzed *atl* mutant synapses with various synaptic markers. For this

purpose, we focused on type Ib boutons formed on muscles 6 and 7 in segment A2. We did not observe any obvious defects in the localization and levels of the presynaptic active zone protein NC82 and the presynaptic vesicle protein CSP in atl^2/Df mutant larvae (Supplementary Fig. S2). We next examined potential structural defects in the postsynaptic side of the NMJ. Type Ib NMJ boutons are surrounded by highly elaborate infoldings of the muscle membrane known as the subsynaptic reticulum (SSR). The fly PDZ protein Dlg has been shown to localize to the SSR and regulate its elaboration during larval development (Budnik et al., 1996). We found that in wild-type third instar larvae, anti-Dlg staining was very intense within the postsynaptic peribouton area, forming a halo-like structure surrounding type Ib boutons (Budnik et al., 1996) (Figs. 3A, A′). In the absence of Atl, the synaptic level of Dlg normalized by HRP intensity was reduced by 36% ($p<0.003$) (Fig. 7A) and barely detected in the peribouton area (Figs. 3B, B′). Interestingly, the total levels of Dlg in body-wall muscles were similar in wild-type and atl^2/Df larvae (data not shown), suggesting that postsynaptic Dlg trafficking and/or stabilization but not expression *per se* might be defective in *atl* mutant muscles. Larvae homozygous for atl^2 also showed a significant reduction in synaptic Dlg levels ($p<0.03$), which was reversed by muscle-specific expression of Atl ($p<0.03$) (Supplementary Fig. S3). The spectrin cytoskeleton is enriched in the pre- and postsynaptic sides of the third instar larval NMJs. In particular, postsynaptic spectrin plays an essential role in the development or integrity of the SSR (Pielage et al., 2006). Therefore, we further examined structural defects of *atl* mutant synapses using an antibody against α-spectrin. In wild-type larvae, α-spectrin staining overlapped with HRP staining and extended well beyond its boundary into the postsynaptic region of the muscle (Fig. 3C). In *atl* mutant larvae, the synaptic level of α-spectrin was reduced by 38% ($p<0.002$) (Fig. 3D). The spectrin signal remaining in mutant NMJs was confined within HRP staining and was barely detected in the peribouton area of the muscle.

The above results strongly suggested that the integrity and/or development of the SSR might be defective in *atl* mutant larvae. To confirm this hypothesis and examine other structural defects, we performed electron microscopy (EM) analyses of type Ib boutons formed on muscles 6 and 7. We found that the cross-sectional midline area of boutons in atl^2/Df was decreased by ~44% compared with wild-type larvae (wild-type: $3.52 \pm 0.25\ \mu m^2$; atl^2/Df: $1.98 \pm 0.12\ \mu m^2$; $p<0.0001$) (Figs. 4A–D). A similar increase in the average size of type Ib boutons was also observed at the light microscopic level (data not shown). EM analyses also revealed that atl^2/Df mutant NMJs often formed small satellite boutons (Fig. 4C). Interestingly, these satellite boutons shared a common SSR with their parental boutons and contained clear synaptic vesicles and T-bars at active zones, suggesting that they may form functional synapses. Despite the change in bouton size, other presynaptic anatomical aspects such as the size and density of synaptic vesicles, the total length and number of active zones per midline cross-section, and T-bar distribution were not significantly changed in atl^2/Df ($p>0.05$) (Table S1).

In the postsynaptic compartment, the SSR in atl^2/Df was conspicuously less extensive than that in wild-type and was also structurally disorganized (Figs. 4A–C). In addition, the boundary between the SSR and muscle-cell cytoplasm was not clearly defined. To quantify the *atl* phenotype in the postsynaptic compartment, we measured SSR thickness (the distance between the presynaptic membrane and the outermost boundary of the SSR), SSR area, and SSR cisterna area. Compared with wild-type, SSR thickness was

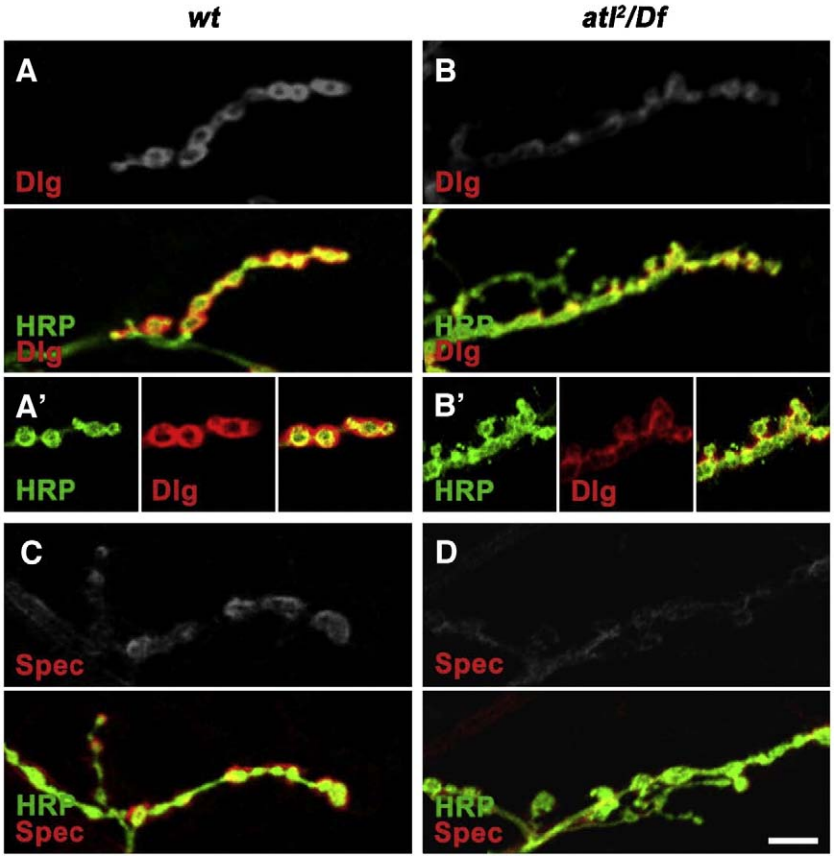

Fig. 3. The synaptic levels of Dlg and α-spectrin are reduced in *atl* mutants. (A, B) Confocal images of wild-type (A) and atl^2/Df (B) larval NMJs 6/7 doubly stained with anti-Dlg (red) and anti-HRP (green) antibodies. Higher magnification images are shown in the bottom panels (A′, B′). (C, D) Confocal images of wild-type (C) and atl^2/Df (D) larval NMJs 6/7 doubly stained with anti-α-spectrin (spec, red) and anti-HRP (green) antibodies. Scale bar: 10 μm.

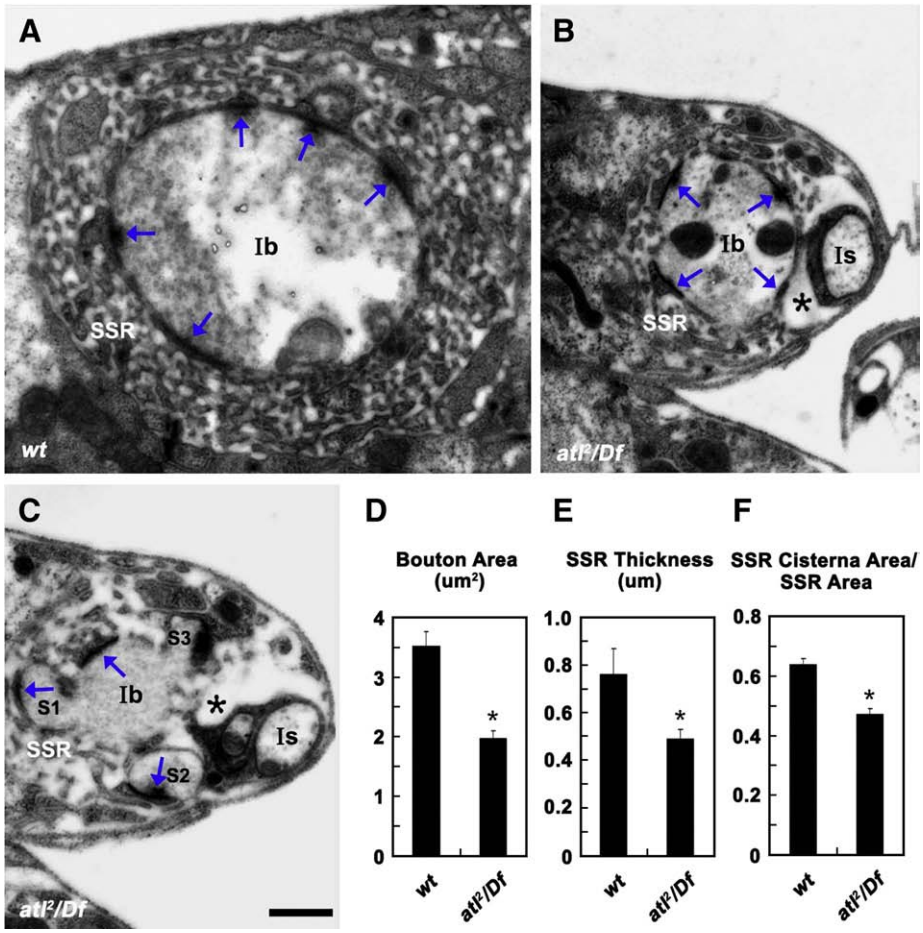

Fig. 4. Ultrastructural analysis of type I NMJ synapses in *atl* mutants. (A–C) Transmission electron micrographs of cross-sectioned type Ib boutons at the third instar larval NMJs 6/7. Arrows mark active zones often decorated with T-bars. (A) A big Ib bouton is completely surrounded by an extensive SSR in a wild-type larva. (B) A small-caliber Ib bouton is surrounded by a disorganized, less extensive SSR in an atl^2/Df mutant larva. (C) An Ib bouton and its satellite boutons (indicated as S1–S3) from the same genotype as (B) are surrounded by a common SSR. Note that some areas of the SSR are devoid of tubular structures in *atl* mutants (indicated by asterisks in [B] and [C]). Type Is boutons are also shown. Scale bar: 500 nm. (D–F) Quantification of the cross-sectional midline bouton area (D), SSR thickness (E), and ratio of SSR cisterna area to SSR area (F). Data are mean ± SEM. Single asterisks indicate statistically significant differences between wild-type ($n=20$) and atl^2/Df ($n=21$) larvae ($p<0.0001$).

reduced by 36% in atl^2/Df (wild-type: 0.76 ± 0.04 μm; atl^2/Df: 0.49 ± 0.04 μm; $p<0.0001$) (Fig. 4E). This change was paralleled by a 53% reduction in the cross-sectional area of the SSR (wild-type: 6.49 ± 0.32 μm^2; atl^2/Df: 3.05 ± 0.31 μm^2; $p<0.0001$) and a 66% reduction in the cross-sectional area of the SSR cisterna (wild-type: 4.20 ± 0.26 μm^2; atl^2/Df: 1.45 ± 0.17 μm^2; $p<0.0001$). Thus, the ratio of the SSR cisterna area to the SSR area was decreased by 27% in atl^2/Df relative to wild-type (wild-type: 0.64 ± 0.02; atl^2/Df: 0.47 ± 0.02; $p<0.0001$) (Fig. 4F), suggesting that *atl* mutations affect SSR organization. In contrast, we found no significant difference in the density of SSR membranes (the number of membrane layers/μm) ($p>0.05$). Overall, our ultrastructural analyses reveal that Atl is required for selective aspects of SSR development.

Atl is required for ER and Golgi morphogenesis in the postsynaptic muscle

To further investigate the cellular function of Atl, we examined its subcellular distribution in muscles. In mammals, Atl-1 is predominantly localized to VTCs and *cis*-Golgi cisternae, while Atl-2 and Atl-3 are highly colocalized with ER markers (Rismanchi et al., 2008; Zhu et al., 2003). We therefore wondered whether *Drosophila* Atl would also be associated with these secretory organelles in vivo. To address this question, we analyzed third instar body-wall muscles expressing either the luminal ER marker Lys-GFP-KDEL or the Golgi marker GalTase-GFP (Snapp et al., 2004). Immunostaining experiments using anti-Atl and anti-GFP antibodies revealed extensive colocalization between Atl and the Lys-GFP-KDEL marker throughout the cytoplasm of muscle cells (Fig. 5A). In contrast, colocalization between Atl and GalTase-GFP was more partial (Fig. 5D). Thus, *Drosophila* Atl localizes primarily to the ER and to a lesser extent, to the Golgi apparatus. As expected from a tight association of ER tubules with microtubules in mammalian cells (Waterman-Storer and Salmon, 1998), Atl signal was also overlapped with microtubules throughout the cytoplasm of muscle cells (Supplementary Fig. S4).

In cultured cells, dominant-negative forms of human Atl-1, Atl-2, and Atl-3 interfere with ER and Golgi morphogenesis (Namekawa et al., 2007; Rismanchi et al., 2008). We examined whether loss of *Drosophila* Atl also produces similar defects. In *atl* mutant muscles, we found a significant reduction in the levels of Lys-GFP-KDEL and GalTase-GFP expression (Figs. 5B, E), suggesting a poor formation of the ER and Golgi apparatus. These phenotypes were partially rescued by muscle-specific expression of Atl (Figs. 5C, F). Thus, data from this study and others support a critical role for Atl and related mammalian proteins in ER and Golgi morphogenesis.

Atl regulates microtubule dynamics

The human Atl-1 protein has been shown to form complexes with the microtubule-severing protein Spastin (Evans et al., 2006;

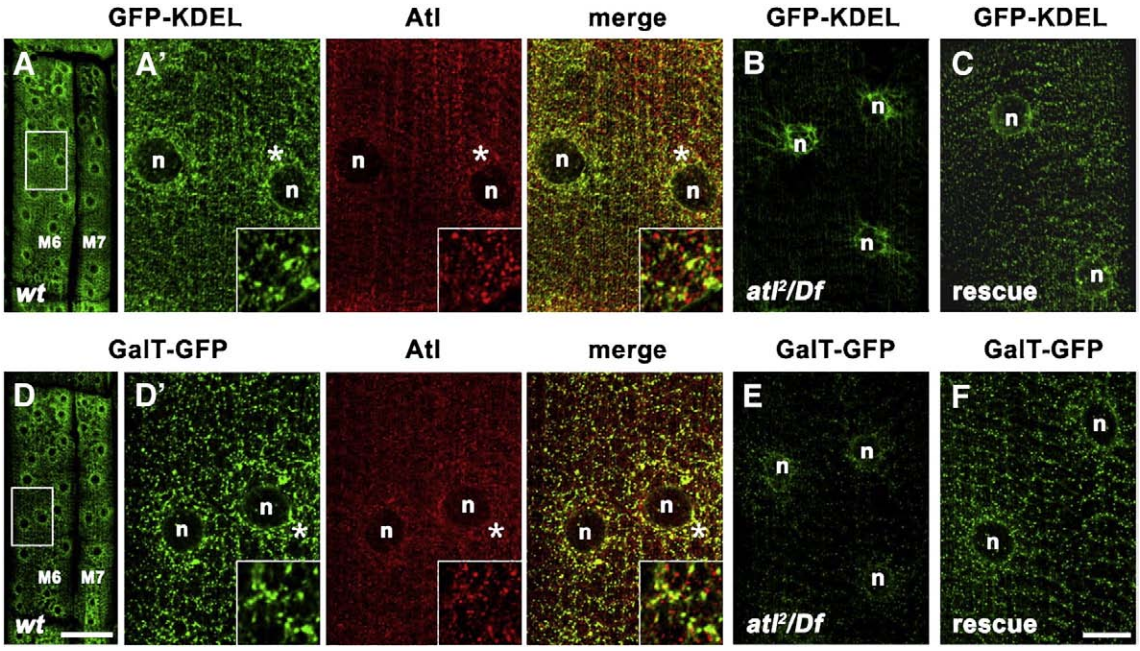

Fig. 5. The endoplasmic reticulum and Golgi apparatus are poorly formed in *atl* mutant muscles. Single confocal sections of muscle cells in wild-type (A, D) and atl^2/Df (B, C, E, F) third instar larvae. Animals were genetically manipulated to express either the luminal ER marker *UAS-Lys-GFP-KDEL* (A–C) or the Golgi marker *UAS-GalTase-GFP* (D–F) under the control of a muscle-specific *BG57-GAL4* driver. In C and F, animals also express *UAS-atl* in the muscle. (A, D) Wild-type muscles doubly stained with anti-GFP (green) and anti-Atl (red). (A′, D′) Higher magnification images of the area indicated by the boxes in A and D. Insets show higher magnification views of the areas marked by asterisks. Atl colocalizes with the ER maker on a reticular network (A′) and partially overlaps with the Golgi marker in a punctate pattern (D′). Anterior is to the top. (B, E) Higher magnification images of atl^2/Df muscles stained with anti-GFP. The levels of the ER (B) and Golgi (E) markers are significantly reduced. (C, F) Higher magnification images of rescued muscles stained with anti-GFP. Muscle-specific expression of Atl partially restores the levels of ER (C) and Golgi (F) markers. n, muscle nuclei. Scale bars: (A, D) 100 μm; (A′, D′, B, C, E, F) 20 μm.

Sanderson et al., 2006). This knowledge, together with the colocalization of Atl and microtubules described above, led us to test whether Atl might be involved in the regulation of microtubule dynamics. For this purpose, we stained the third instar body-wall muscles with an anti-α-tubulin antibody, which preferentially detects polymerized tubulin rather than free tubulin dimers (Sherwood et al., 2004). In wild-type larvae, a complex network of microtubules was detected along the muscle axes with particular enrichment around muscle nuclei (Fig. 6A). The body-wall muscles in atl^2/Df larvae contained more prominent microtubules than those in wild-type muscles (Fig. 6B). The total level of α-tubulin monomers in atl^2/Df larval muscles was similar to that in wild-type muscles (Fig. 6E). Thus, the kinetics of microtubule assembly and/or disassembly are altered in *atl* mutant muscles, which in turn results in the accumulation of microtubules. To confirm the role of Atl in the regulation of microtubule dynamics, we also visualized microtubules in wild-type muscles overexpressing Atl. We found a significant reduction of microtubules in these muscles compared to the wild-type muscles (Fig. 6C). In contrast, overexpression of a dominant-negative form of Atl (Atl^{R192Q}) in wild-type muscles produced a mild, but highly reproducible, increase in α-tubulin staining intensity (Fig. 6D). In a control experiment, the organization and levels of actin filaments in myofibrils were not changed by the dosage level of Atl, as visualized with phalloidin (Figs. 6A–D). Taken together, our data reveal that Atl regulates microtubule dynamics in the muscle.

We also examined presynaptic microtubules at NMJ 6/7 in atl^2/Df larvae. For this purpose, we used an antibody (mAb 22C10) against the MAP1B-like protein Futsch to label stable microtubules (Hummel et al., 2000; Roos et al., 2000). In wild-type larvae, Futsch staining revealed bundled microtubules within motor axons and NMJ branches infiltrating some boutons. The intensity and pattern of Futsch staining in atl^2/Df larvae were not significantly different from those in wild-type larvae (Supplementary Figs. S5A, B). We also examined wild-type larvae overexpressing Atl in neurons, but could not find abnormalities in the level and pattern of presynaptic microtubules (Supplementary Fig. S5C). To quantify these data, we compared the percentage of NMJ 6/7 boutons containing detectable levels of Futsch in wild-type, atl^2/Df, and Atl-overexpressing larvae, but observed no significant difference (Supplementary Fig. S5D).

Atl functionally interacts with Spastin

In *Drosophila* larval muscles, overexpression of Spastin results in a decrease of microtubule networks, while loss or reduction of Spastin has the opposite effect on them (Orso et al., 2005; Sherwood et al., 2004; Trotta et al., 2004). Thus, the effect of Spastin dosage on muscle microtubules is essentially identical to that of *atl*. To provide additional evidence for the similarity of the *spastin* and *atl* loss-of-function muscle phenotypes, we examined the levels of ER and Golgi markers in the muscle of $spas^{5.75}$, a previously reported *spastin*-null allele (Sherwood et al., 2004). We observed a significant reduction of Lys-GFP-KDEL and GalT-GFP expression (Supplementary Fig. S6), which is reminiscent of the *atl* mutant phenotype. Thus, phenotypic overlap between *atl* and *spastin* provides genetic support that they could be functionally inter-related in the muscle.

To directly test the relationship between Atl and Spastin, we first proved physical interaction between Atl and an N-terminal region of Spastin (amino acids 1–159) by GST pull-down assays (Fig. 7A). We then examined whether loss of *spastin* function could suppress *atl* gain-of-function phenotypes. In addition to a dramatic reduction in microtubules as described above (Fig. 6C), muscle-specific overexpression of Atl in a wild-type background at 25 °C often led to partial or complete detachment of muscles from their attachment sites, producing defects in muscle shape (Figs. 7B, C). Moreover, we observed a significant decrease in the staining intensity of acetylated α-tubulin (Figs. 7F, G), a posttranslationally modified α-tubulin that is

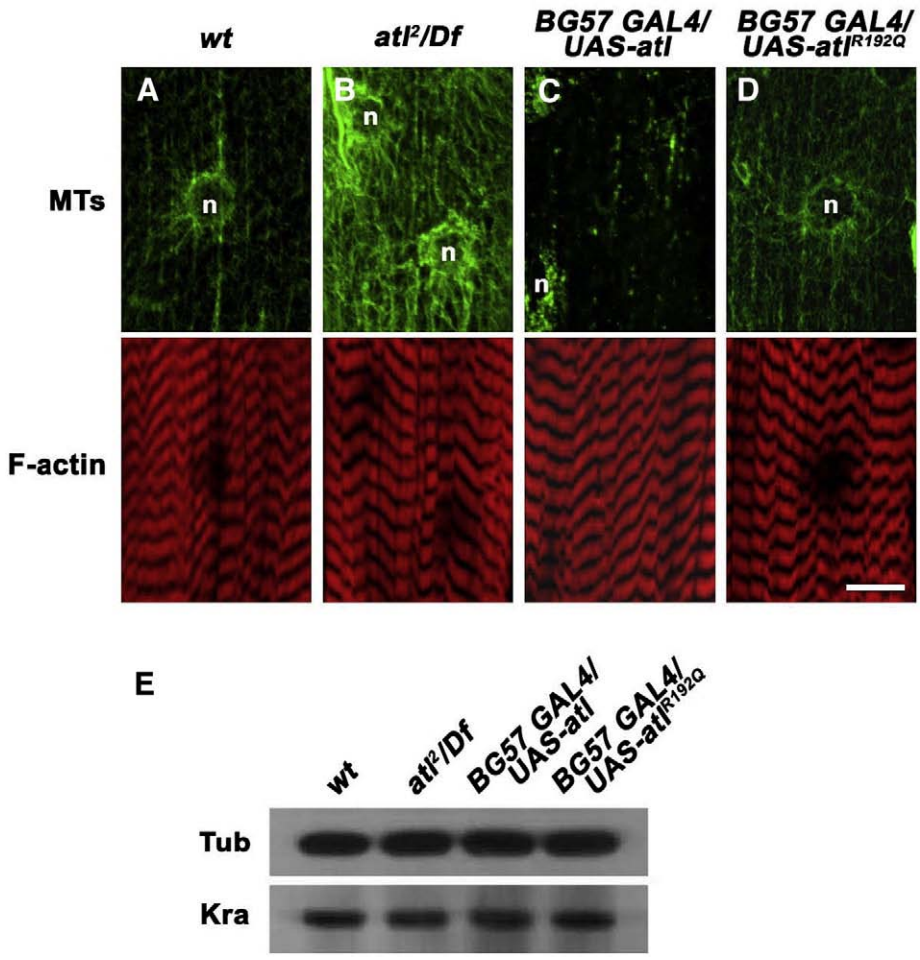

Fig. 6. Atl regulates microtubule dynamics in the postsynaptic muscle. (A–D) Third instar larval muscles doubly stained with anti-α-tubulin (green) and phalloidin (red) to visualize microtubules (MTs) and filamentous actin (F-actin), respectively. The genotypes analyzed were wild-type (A), atl^2/Df (B), *BG57-GAL4/UAS-atl* (C), and *BG57-GAL4/UAS-atl*^{R192Q} (D). Abundance of microtubules is inversely related to the dosage levels of Atl, while the levels and organization of F-actin within myofibrils are not influenced by Atl dosage changes. n, muscle nuclei. Scale bar: 20 μm. (E) Western blot analysis of larval muscle extracts using anti-α-tubulin antibody. The same blot was reprobed with anti-Kra antibody (Lee et al., 2007) to confirm equal protein loading.

present only in stable microtubules (Hubbert et al., 2002). These gain-of-function phenotypes were significantly suppressed by removing both copies of *spastin* (Figs. 7D, H). *spastin* mutation ($spas^{5.75}$) alone did not disturb the pattern of muscle morphology at detectable levels (Fig. 7E). However, it led to an increase in the acetylated α-tubulin staining intensity in the muscle (Fig. 7I), as previously reported (Orso et al., 2005). Thus, our biochemical and genetic data suggest that Atl and Spastin function together to regulate microtubule stability and other biological processes.

Vinblastine attenuates atl loss-of-function phenotypes

To further investigate the relationship between microtubule misregulation and other phenotypes observed in *atl* mutants, we examined whether pharmacological suppression of microtubule accumulation in *atl* mutant larvae could rescue key aspects of *atl* loss-of-function phenotypes. We found that feeding atl^2/Df mutant animals with 1 μM vinblastine restored the level of microtubules in larval muscles close to wild-type (data not shown). This change was accompanied by increases in the levels of the Lys-GFP-KDEL and GalT-GFP markers (Supplementary Fig. S7). In addition, vinblastine treatment reversed the reduction in the synaptic level of Dlg, the increase in bouton number, and the decrease in muscle size (Figs. 8A–D). In a control experiment, administration of vinblastine to wild-type animals did not produce statistically significant changes in NMJ or muscle growth (Figs. 8A–D). Finally, treatment of atl^2/Df mutant animals with 0.1 μM vinblastine resulted in a significant increase in adult viability (Fig. 8E). Taken together, our data suggest that microtubule misregulation is a causative mechanism leading to the abnormalities in synapse development and ER and Golgi morphogenesis and the lethality in *atl* mutants.

Discussion

Mutations in the human *atl* (SPG3A) gene cause the second most common form of HSP (Fink, 2003). However, our knowledge about the pathogenesis of HSP SPG3A is still very limited, mainly because the precise cellular functions of atlastin-subfamily GTPases have not been determined. In this paper, we provide evidence that *Drosophila* Atl functions with Spastin in the same pathway to disassemble muscle microtubules and that this regulation is critical for synapse development at the NMJ and ER and Golgi morphogenesis in the muscle.

Atl functions in the postsynaptic muscle to regulate synapse development

During *Drosophila* larval development, there is a coordinated growth of the muscle and NMJ (Schuster et al., 1996). Our re-

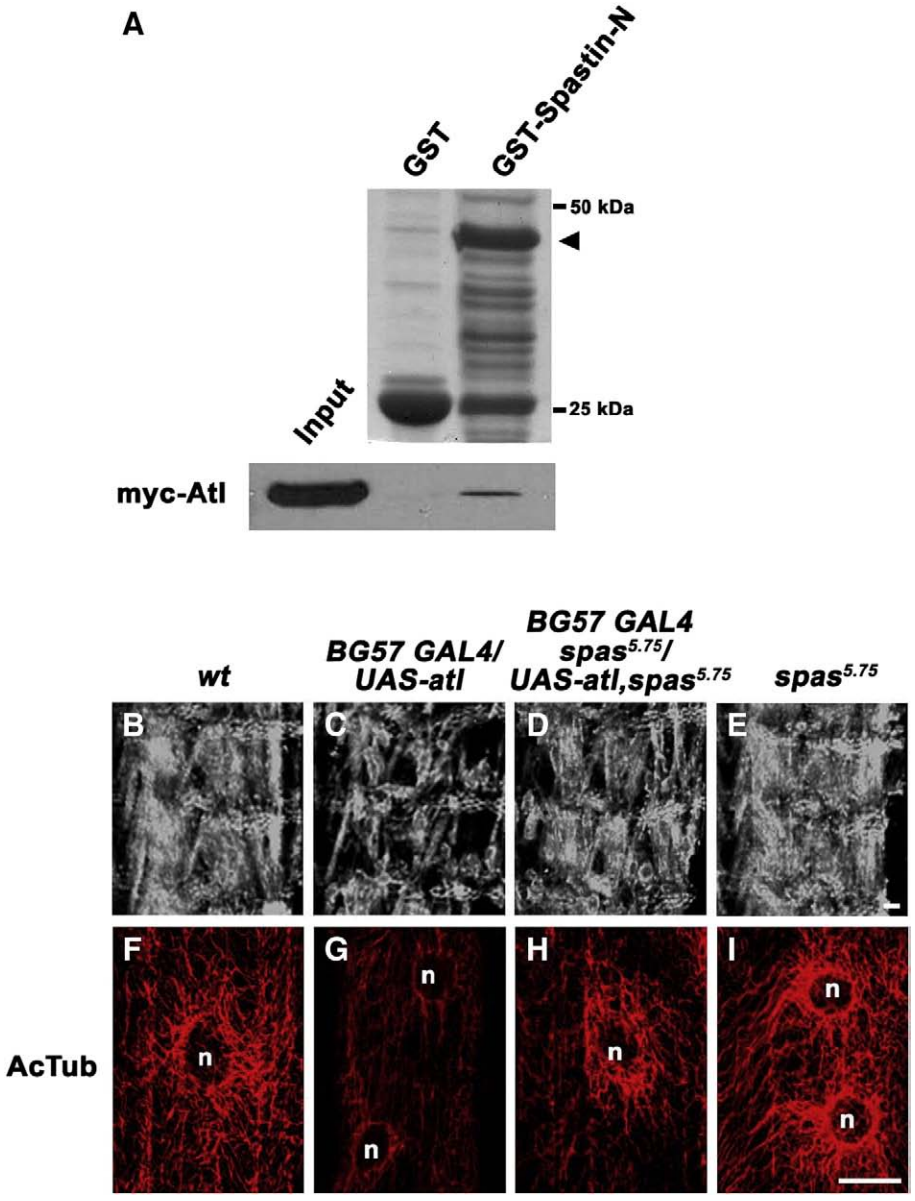

Fig. 7. Atl interacts physically and functionally with Spastin. (A) Atl interacts with Spastin in vitro. In pull-down assays, GST-Spastin-N (amino acids 1–159) or GST was incubated with cell lysate from HEK293 cells transiently expressing Myc-tagged Atl. An SDS-gel stained with Coomassie Blue shows the amounts of GST and GST-Spastin-N (an arrowhead) used for pull-down assays (top panel). The presence of Myc-Atl in the precipitates was detected by western blot analysis using anti-Myc (bottom panel). Input, 10% of the input amount of Myc-Atl used in each reaction. (B–I) *atl* gain-of-function muscle phenotypes are suppressed by *spastin*-null mutation. The genotypes analyzed are wild-type (B, F), *BG57-GAL4/UAS-atl* (C, G), *BG57-GAL4,spas*$^{5.75}$*/UAS-atl,spas*$^{5.75}$ (D, H), and *spas*$^{5.75}$*/spas*$^{5.75}$ (E, I). (B–E) Third instar larval fillets were examined using Nomarski optics. Two abdominal hemisegments (A2 and A3) are shown. Anterior is to the top. (F–I) High magnification confocal images are shown for muscle 6 in abdominal segment 2 stained with anti-acetylated-α-tubulin. n, muscle nuclei. Scale bars: (B–E) 100 μm; (F–I) 20 μm.

sults suggest that these developmental processes are impaired in the absence of Atl. In *atl* mutant larvae, NMJ boutons are smaller and more numerous than in wild-type larvae. In addition, the size of body-wall muscles is significantly reduced. These phenotypes are rescued by muscle-specific expression of Atl, suggesting that Atl functions primarily in the postsynaptic muscle to control NMJ synapse and muscle growth. This conclusion is further supported by our observation that targeted expression of a dominant-negative form of Atl (Atl^{R192Q}) in muscles, but not in neurons, mimics *atl* mutations to increase bouton number per muscle surface area.

In *Drosophila*, type I NMJ boutons are surrounded by the SSR, which is highly elaborated infoldings of the muscle membrane. The SSR begins to form during the first larval instar and increases in size and complexity throughout late larval life (Guan et al., 1996). Our ultrastructural analysis indicates that the SSR is less extensive and disorganized in *atl* mutants. Consistent with this finding, we observe defects in the levels and distribution of Dlg and spectrin, the synaptic scaffold proteins that play critical roles for SSR expansion and organization (Budnik et al., 1996; Guan et al., 1996; Pielage et al., 2006). Thus, our results suggest that Atl is required for the formation and/or maintenance of normal postsynaptic structure.

Atl regulation of muscle microtubules

In mammals, there are three members of the atlastin subfamily of large GTPases, each with a distinct tissue distribution. In particular, Atl-1 is primarily enriched in the CNS (Zhu et al., 2003), while Atl-2 and Atl-3 are highly expressed in muscle tissues (Rismanchi et al.,

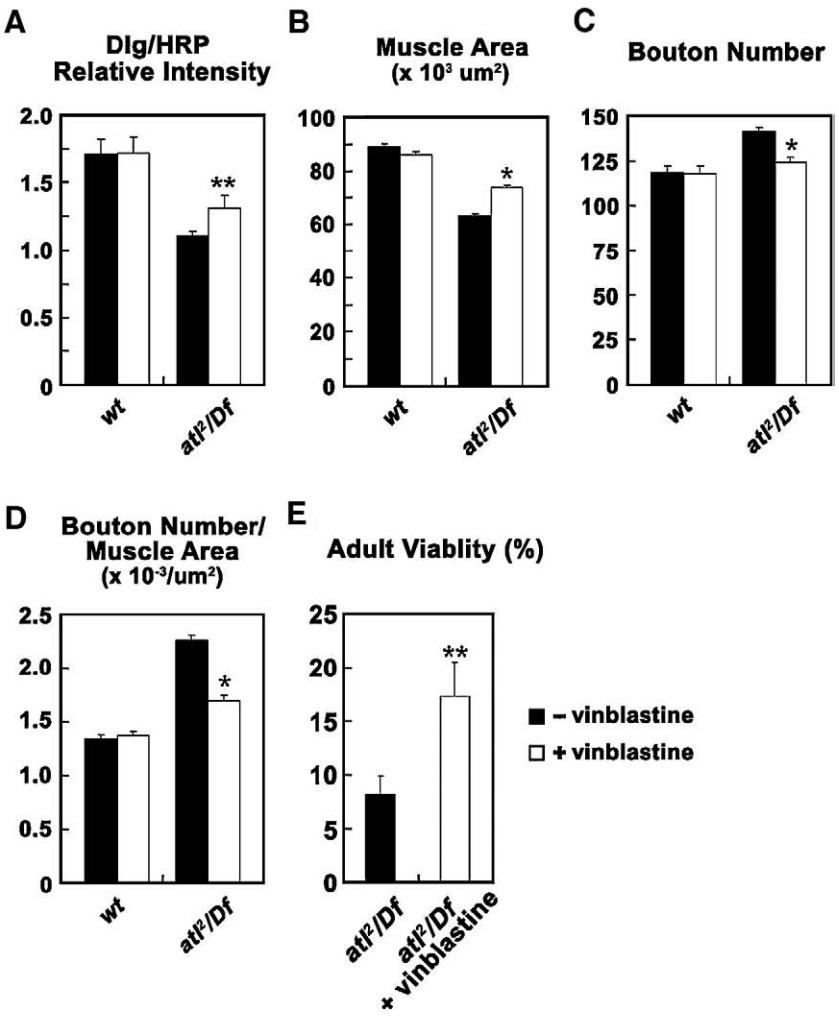

Fig. 8. *atl* loss-of-function phenotypes are suppressed by administration of vinblastine. (A–D) Quantification of the Dlg/HRP relative intensity (A), the combined surface area of muscles 6 and 7 (B), bouton number (C), and bouton number normalized to muscle surface area (D) in wild-type ($n>8$) and atl^2/Df ($n>20$) larvae. Animals were raised in the absence or presence of 1 μM vinblastine, and larval NMJs formed on muscles 6 and 7 in abdominal segment A2 were analyzed. Vinblastine treatment partially rescues defects in the levels of Dlg, bouton number, and muscle size caused by *atl* mutations. (E) Rescue of the atl^2/Df lethality by adding 0.1 μM vinblastine to the food. Data are mean ± SEM. Statistically significant changes induced by vinblastine treatment are denoted by an asterisk ($p<0.0001$) and double asterisk ($p<0.05$).

2008). This expression profile of mammalian atlastins suggests the possibility that they may play an essential role in both pre- and postsynaptic cells. In *Drosophila*, the single ortholog of mammalian atlastins (Atl) is expressed in the adult brain and is required for maintaining dopaminergic neurons (Lee et al., 2008). In this study, we investigated the cellular function of Atl in the developing postsynaptic muscle.

In muscle cells, loss of Atl produces abnormal accumulation of stable microtubules, while its overexpression has the opposite effect. Thus, our genetic experiments reveal for the first time that Atl is involved in normal disassembly of microtubules. However, Atl is not homologous to any known microtubule-associated proteins, raising the key question as to how Atl regulates microtubule stability. Genetic and biochemical data obtained from this study and others support the model in which Atl acts through Spastin to disassemble microtubules. First, phenotypic overlap between *atl* and *spastin* is very extensive in *Drosophila*. *atl* and *spastin* mutants display similar adult phenotypes: short life span, impairments in locomotor activity, and age-dependent neurodegeneration (Lee et al., 2008; Orso et al., 2005; Sherwood et al., 2004). *spastin* mutations are also shown to cause an increase in bouton number and satellite bouton formation at larval NMJs (Sherwood et al., 2004). This study demonstrates that NMJ morphology is similarly affected by *atl* mutations. Moreover, we show that both mutations lead to a decrease in expression of ER and Golgi markers in muscle cells. Second, we demonstrate that Atl and Spastin can physically bind each other in vitro. Finally, we show that *spastin*-null mutation suppresses the loss of stable microtubules induced by *atl* overexpression.

How is Atl involved in Spastin-mediated microtubule disassembly? Proteins in the AAA family have been shown to maintain their substrate specificities often by biochemical interactions with adaptor proteins that can bring them to specific subcellular compartments or molecular targets (Dougan et al., 2002). Potential adaptor proteins for mammalian Spastin include a centrosomal protein NA14 (Errico et al., 2004) and an endosomal protein CHMP1B (Reid et al., 2005), suggesting that Spastin may function at multiple subcellular compartments. We show here that Atl in the *Drosophila* muscle localizes largely to the ER and partially to the Golgi apparatus. Together with biochemical interactions between Spastin and Atl, this result raises the possibility that Atl may function as an ER- and Golgi-specific adaptor for Spastin in the muscle. However, we cannot exclude the possibility that Atl may modulate the microtubule-severing activity or stability of Spastin. Future work is needed to address this issue.

Atl mode of action in ER and Golgi morphogenesis and synapse development

Dominant-negative or pathogenic forms of mammalian atlastins interfere with the formation, migration, or fusion of vesicles in the ER/Golgi interface in cultured cells (Namekawa et al., 2007) and disrupt the morphology of these organelles (Namekawa et al., 2007; Rismanchi et al., 2008). Our study provides in vivo evidence that *Drosophila* Atl is required for normal formation of the ER and Golgi organelles. Thus, data obtained from mammalian cells and *Drosophila* support the role for Atl and its mammalian homologs in membrane trafficking from the ER and morphogenesis of the ER and Golgi apparatus. What is then the relationship between microtubule stability and morphogenesis of the ER and Golgi morphogenesis? Two lines of our evidence suggest that Atl-dependent microtubule disassembly is critical for normal morphogenesis of those organelles. First, *spastin*-null mutants display ER and Golgi defects similar to those in *atl* mutants. Second, the ER and Golgi phenotype in *atl* is significantly rescued by administration of the microtubule-destabilizing drug vinblastine. Thus, accumulation of stable microtubules appears to be a causative mechanism to account for defects in ER and Golgi morphogenesis in *atl*. This conclusion is compatible with the previously reported roles for the microtubule cytoskeleton in membrane trafficking between the ER and the Golgi apparatus (Lippincott-Schwartz et al., 1995; Mizuno and Singer, 1994), as well as in the organization and distribution of those secretory organelles (Ralston et al., 1999; Waterman-Storer and Salmon, 1998).

The postsynaptic defects of *atl* mutants are also rescued by pharmacologically reversing microtubule accumulation, raising an important question as to how the lack of Atl-mediated microtubule regulation induces abnormalities in postsynaptic structure. One possibility is that defects in vesicle trafficking induced by *atl* mutations could impair the delivery of synaptic membrane components, which in turn would produce an underdeveloped and disorganized SSR. If this is the case, Atl-mediated microtubule regulation may be critical for "Golgi-bypass" secretory pathways since anterograde ER-to-Golgi protein trafficking appears to be normal in cells expressing dominant-negative forms of atlastins (Rismanchi et al., 2008). Such pathways include a Rab1-positive route that connects the pre-Golgi intermediate compartment (IC) directly with the cell periphery (Sannerud et al., 2006). In this regard, it will be interesting to address in the future whether synaptic components critical for SSR development are transported to the plasma membrane through the Rab1-mediated or related pathways in the muscle. An alternative and additional possibility is that loss of Atl could alter local microtubules surrounding the postsynaptic area, thereby affecting SSR structure. At the *Drosophila* NMJ, muscle microtubules are excluded from the peribouton area (i.e. SSR) that can be defined by the spectrin/actin network (Ruiz-Canada et al., 2004). It has been proposed that the extent of the SSR is strongly correlated with postsynaptic aPKC activity, which decreases the stability of muscle microtubules (Ruiz-Canada et al., 2004). By analogy with aPKC, Atl could support the expansion of the SSR by decreasing the stability of local microtubules surrounding the SSR. At this time, however, we cannot exclude other mechanisms by which misregulation of muscle microtubules may alter the postsynaptic structure, as observed in the postsynaptic side of *atl* mutant NMJs.

At present, it is still unclear how postsynaptic Atl regulates presynaptic growth. Since over-activation of retrograde BMP signaling also produces an NMJ phenotype characterized primarily by increased satellite bouton formation at the NMJ, it is an open question whether microtubule misregulation in *atl* inhibits the activity or the secretion from postsynaptic muscles of BMP and other retrograde growth signals.

Implications for the developmental role of HSP proteins

The HSP proteins implicated in microtubule organization and/or microtubule-dependent processes include microtubule motor protein KIF5A and other molecules containing the microtubule interacting and trafficking (MIT) domain (e.g., Spartin and Spastin). Previous functional characterization of these proteins has centered on their roles in axons and presynaptic terminals. For example, Spastin has been shown to be expressed at the presynaptic compartment of the *Drosophila* larval NMJ, and to regulate synaptic structure and function by regulating the stability of presynaptic microtubules (Sherwood et al., 2004; Trotta et al., 2004). However, the Spastin protein is also expressed in the postsynaptic muscle in *Drosophila* and humans (Hazan et al., 1999; Trotta et al., 2004). At present, it is unknown to what extent microtubule misregulation in the postsynaptic cell contributes to the presynaptic phenotypes observed in *Drosophila spastin*-null mutants and human patients with HSP SPG4. We have clearly demonstrated in *Drosophila* that misregulation of muscle microtubules caused by *atl* mutations produces synaptic defects, highly reminiscent of those seen with *spastin* loss-of-function mutations. Given the biochemical and functional links between Atl and Spastin, the current work provides a new perspective on the postsynaptic role of Spastin and other microtubule-related HSP proteins during synapse development.

Materials and methods

Fly stocks

atl^1 (a P-element insertion in the *atl* locus) and transgenic flies carrying *atl-Ge* (a genomic fragment covering the *atl* gene), *UAS-atl*, or *UAS-atl* ^{R192Q} have been previously described (Lee et al., 2007). The atl^2 mutant was generated by imprecise excision of atl^1. *Df(3R) Exel7357* (a deficiency that removes the *atl* locus) and *elav-GAL4* were obtained from the *Drosophila* Bloomington Stock Center. *UAS-Lys-GFP-KDEL* and *UAS-GalT-GFP* transgenics were obtained from Dr. Mary A. Lilly (Snapp et al., 2004); *Casper-MHC-CD8-GFP-Shaker* was a gift from Dr. Ehud Y. Isacoff (Zito et al., 1999); and *BG57-GAL4* was provided by Dr. Young-Ho Koh (Budnik et al., 1996).

Flies were maintained at 25 °C on standard *Drosophila* food unless otherwise noted. For some experiments, experimental crosses were performed at 18 °C. To analyze the phenotypic consequences of feeding flies with vinblastine, flies were grown on standard food containing 1 μM vinblastine sulfate (Sigma).

Antibodies

To produce an antibody against Atl, *atl* cDNA encoding amino acids 1–421 was subcloned in frame into the pGEX6P1 expression vector (Amersham Pharmacia). The GST-Atl fusion protein was purified with glutathione-Sepharose 4B (Amersham Pharmacia) and digested with PreScission protease (Amersham Pharmacia). The band representing cleaved Atl was excised from SDS-PAGE gels for the immunization of rats. The resulting antiserum was purified with MBP-tagged Atl (amino acids 1–421) fusion protein which was crosslinked to CNBr-activated Sepharose 4 Fast Flow (Amersham Pharmacia). This purified antibody was used at a dilution of 1:500 for western blotting and 1:50 for immunohistochemistry.

For immunohistochemistry, the following antibodies were purchased from the Developmental Studies Hybridoma Bank: anti-Dlg mAb 4F3 (1:400), anti-Csp3 mAb 1G12 (1:250), anti-Bruchpilot mAb NC82 (1:10), and anti-Futsch mAb 22C10 (1:50). Other antibodies used in this study include mouse anti-α-tubulin (1:500, Sigma), mouse anti-acetylated α-tubulin (1:500, Sigma), rat anti-tyrosinated α-tubulin (1:40, Chemicon), rabbit anti-GFP (1:250, Abcam), goat FITC-conjugated anti-HRP (1:200, Jackson Laboratories), and donkey

FITC or Cy3-conjugated secondary antibodies (1:200, Jackson Laboratories).

Western blot analysis

Larval body-wall muscles were homogenized in 1 × SDS sample buffer, subjected to SDS-PAGE, and transferred to nitrocellulose membranes (Whatman). Blots were blocked in 5% skim milk/TBST (TBS, 0.2% Tween-20) and incubated with primary antibodies in 5% skim milk/TBST overnight at 4 °C. After several washes in TBST, blots were incubated for 1 h with HRP-conjugated secondary antibodies in 5% skim milk/TBST. Blots were washed several times with TBST and visualized with SuperSignal West Pico CL substrate (Pierce). Antibodies were used at the following dilutions: anti-Dlg (1:4000), anti-Kra (1:4000) (Lee et al., 2007), anti-α-tubulin (1:4000), anti-β-actin (1:1000), and HRP-conjugated secondary antibodies (1:5000, Jackson Laboratories).

Immunohistochemistry

Wandering third instar larvae were dissected in Ca^{2+}-free HL3 saline (5 mM HEPES [pH 7.2], 70 mM NaCl, 5 mM KCl, 20 mM $MgCl_2$, 10 mM $NaHCO_3$, 5 mM trehalose, 115 mM sucrose) (Stewart et al., 1994) and fixed in 4% formaldehyde/PBS for 30 min. Fixed larvae were washed in PBT (PBS, 0.1% Triton X-100), blocked with 5% BSA/PBT for 1 h, and incubated with primary antibodies at 4 °C overnight. After several washes with PBT, dissections were incubated with secondary antibodies for 1 h at room temperature. Fluorescence images were collected under an Olympus FV300 confocal microscope using Olympus FLUOVIEW software. Samples were processed simultaneously with controls in the same tube and imaged at identical confocal settings. Images shown in Figs. 1F–H, 3, 5, 6A–D, 7B–I, S1, S2, S3A–C, S4, S6, and S7 are single confocal sections, and the other images were made by projections of z series stacks with 1 μm intervals. Fluorescence intensity was determined using Olympus FLUOVIEW (version 5.0) image analysis software. Muscle surface area was visualized by saturating HRP signal and measured using the Olympus FLUOVIEW software. Quantification of immunochemistry was obtained by normalizing the fluorescence intensity of Dlg to that of HRP.

Electron microscopy

Third instar larvae were dissected in Ca^{2+}-free HL3 saline and fixed for 2 h at 4 °C in 4% paraformaldehyde/2.5% glutaraldehyde/0.1 M phosphate buffer (PB, pH 7.4). After rinsing with 0.1 M PB, the specimens were osmicated with 1% OsO_4/0.1 M PB for 1 h, dehydrated in graded alcohols, flat-embedded in Durcupan ACM (Fluka), and cured for 48 h at 60 °C. Transverse ultrathin serial sections (80–90 nm) were cut from muscles 6 and 7 at the second abdominal segment. The sections were mounted on formvar-coated single slot grids, stained with uranyl acetate and lead citrate, and examined with a Hitachi H-7500 electron microscope (Hitachi) at 80 kV accelerating voltage. Images of type Ib boutons were captured at 25,000× using Gatan Digitalmicrograph software driving a SC1000 CCD camera (Orius). The largest diameter section representing the bouton midline was used for quantitative analysis using NIH Image J 1.38. Three preparations were analyzed for w^{1118} (a wild-type control) and atl^2/*Df*. Morphometric analyses of synaptic boutons and the SSR were performed as described in Budnik et al. (1996).

Acknowledgments

We thank Dr. Jaesang Kim for comments on the manuscript. We are grateful to Drs. Mary A. Lilly, Young-Ho Koh, Nina T. Sherwood, and Jaeseob Kim for fly stocks. This work was supported by grants from the Research Program for New Drug Target Discovery (M10748000283-07N4800-28310), the Brain Research Center of the 21st Century Frontier (M103KV010002-06K2201-00210), the Basic Research Program of the Korea Science and Engineering Foundation (R01-2006-000-10487-0), and the Korea Research Foundation (KRF-2006-312-C00361).

Appendix A. Supplementary data

Supplementary data associated with this article can be found, in the online version, at doi:10.1016/j.ydbio.2009.03.019.

References

Brand, A.H., Perrimon, N., 1993. Targeted gene expression as a means of altering cell fates and generating dominant phenotypes. Development 118, 401–415.
Budnik, V., Koh, Y.H., Guan, B., Hartmann, B., Hough, C., Woods, D., Gorczyca, M., 1996. Regulation of synapse structure and function by the *Drosophila* tumor suppressor gene dlg. Neuron 17, 627–640.
Dougan, D.A., Mogk, A., Zeth, K., Turgay, K., Bukau, B., 2002. AAA+ proteins and substrate recognition, it all depends on their partner in crime. FEBS Lett. 529, 6–10.
Errico, A., Claudiani, P., D'Addio, M., Rugarli, E.I., 2004. Spastin interacts with the centrosomal protein NA14, and is enriched in the spindle pole, the midbody and the distal axon. Hum. Mol. Genet. 13, 2121–2132.
Evans, K., Keller, C., Pavur, K., Glasgow, K., Conn, B., Lauring, B., 2006. Interaction of two hereditary spastic paraplegia gene products, spastin and atlastin, suggests a common pathway for axonal maintenance. Proc. Natl. Acad. Sci. U. S. A. 103, 10666–10671.
Fink, J.K., 2003. Advances in the hereditary spastic paraplegias. Exp. Neurol. 184, S106–S110.
Guan, B., Hartmann, B., Kho, Y.H., Gorczyca, M., Budnik, V., 1996. The *Drosophila* tumor suppressor gene, dlg, is involved in structural plasticity at a glutamatergic synapse. Curr. Biol. 6, 695–706.
Harding, A.E., 1983. Classification of the hereditary ataxias and paraplegias. Lancet 1, 1151–1155.
Hazan, J., Fonknechten, N., Mavel, D., Paternotte, C., Samson, D., Artiguenave, F., Davoine, C.S., Cruaud, C., Durr, A., Wincker, P., Brottier, P., Cattolico, L., Barbe, V., Burgunder, J.M., Prud'homme, J.F., Brice, A., Fontaine, B., Heilig, B., Weissenbach, J., 1999. Spastin, a new AAA protein, is altered in the most frequent form of autosomal dominant spastic paraplegia. Nat. Genet. 23, 296–303.
Hubbert, C., Guardiola, A., Shao, R., Kawaguchi, Y., Ito, A., Nixon, A., Yoshida, M., Wang, X.F., Yao, T.P., 2002. HDAC6 is a microtubule-associated deacetylase. Nature 417, 455–458.
Hummel, T., Krukkert, K., Roos, J., Davis, G., Klambt, C., 2000. *Drosophila* Futsch/22C10 is a MAP1B-like protein required for dendritic and axonal development. Neuron 26, 357–370.
Jan, L.Y., Jan, Y.N., 1982. Antibodies to horseradish peroxidase as specific neuronal markers in *Drosophila* and in grasshopper embryos. Proc. Natl. Acad. Sci. U. S. A. 79, 2700–2704.
Lee, S., Nahm, M., Lee, M., Kwon, M., Kim, E., Zadeh, A.D., Cao, H., Kim, H.J., Lee, Z.H., Oh, S.B., Yim, J., Kolodziej, P.A., 2007. The F-actin-microtubule crosslinker Shot is a platform for Krasavietz-mediated translational regulation of midline axon repulsion. Development 134, 1767–1777.
Lee, Y., Paik, D., Bang, S., Kang, J., Chun, B., Lee, S., Bae, E., Chung, J., Kim, J., 2008. Loss of spastic paraplegia gene atlastin induces age-dependent death of dopaminergic neurons in *Drosophila*. Neurobiol. Aging 29, 84–94.
Lippincott-Schwartz, J., Cole, N.B., Marotta, A., Conrad, P.A., Bloom, G.S., 1995. Kinesin is the motor for microtubule-mediated Golgi-to-ER membrane traffic. J. Cell Biol. 128, 293–306.
McDermott, C.J., Grierson, A.J., Wood, J.D., Bingley, M., Wharton, S.B., Bushby, K.M., Shaw, P.J., 2003. Hereditary spastic paraparesis: disrupted intracellular transport associated with spastin mutation. Ann. Neurol. 54, 748–759.
Mizuno, M., Singer, S.J., 1994. A possible role for stable microtubules in intracellular transport from the endoplasmic reticulum to the Golgi apparatus. J. Cell Sci. 107, 1321–1331.
Namekawa, M., Ribai, P., Nelson, I., Forlani, S., Fellmann, F., Goizet, C., Depienne, C., Stevanin, G., Ruberg, M., Durr, A., Brice, A., 2006. SPG3A is the most frequent cause of hereditary spastic paraplegia with onset before age 10 years. Neurology 66, 112–114.
Namekawa, M., Muriel, M.P., Janer, A., Latouche, M., Dauphin, A., Debeir, T., Martin, E., Duyckaerts, C., Prigent, A., Depienne, C., Sittler, A., Brice, A., Ruberg, M., 2007. Mutations in the SPG3A gene encoding the GTPase atlastin interfere with vesicle trafficking in the ER/Golgi interface and Golgi morphogenesis. Mol. Cell. Neurosci. 35, 1–13.
Orso, G., Martinuzzi, A., Rossetto, M.G., Sartori, E., Feany, M., Daga, A., 2005. Disease-related phenotypes in a *Drosophila* model of hereditary spastic paraplegia are ameliorated by treatment with vinblastine. J. Clin. Invest. 115, 3026–3034.
Pielage, J., Fetter, R.D., Davis, G.W., 2006. A postsynaptic spectrin scaffold defines active zone size, spacing, and efficacy at the *Drosophila* neuromuscular junction. J. Cell Biol. 175, 491–503.
Praefcke, G.J., McMahon, H.T., 2004. The dynamin superfamily: universal membrane tubulation and fission molecules? Nat. Rev. Mol. Cell. Biol. 5, 133–147.

Ralston, E., Lu, Z., Ploug, T., 1999. The organization of the Golgi complex and microtubules in skeletal muscle is fiber type-dependent. J. Neurosci. 19, 10694–10705.
Reid, E., 2003. Science in motion: common molecular pathological themes emerge in the hereditary spastic paraplegias. J. Med. Genet. 40, 81–86.
Reid, E., Connell, J., Edwards, T.L., Duley, S., Brown, S.E., Sanderson, C.M., 2005. The hereditary spastic paraplegia protein spastin interacts with the ESCRT-III complex-associated endosomal protein CHMP1B. Hum. Mol. Genet. 14, 19–38.
Rismanchi, N., Soderblom, C., Stadler, J., Zhu, P.P., Blackstone, C., 2008. Atlastin GTPases are required for Golgi apparatus and ER morphogenesis. Hum. Mol. Genet. 17, 1591–1604.
Roos, J., Hummel, T., Ng, N., Klambt, C., Davis, G.W., 2000. *Drosophila* Futsch regulates synaptic microtubule organization and is necessary for synaptic growth. Neuron 26, 371–382.
Ruiz-Canada, C., Ashley, J., Moeckel-Cole, S., Drier, E., Yin, J., Budnik, V., 2004. New synaptic bouton formation is disrupted by misregulation of microtubule stability in aPKC mutants. Neuron 42, 567–580.
Sanderson, C.M., Connell, J.W., Edwards, T.L., Bright, N.A., Duley, S., Thompson, A., Luzio, J.P., Reid, E., 2006. Spastin and atlastin, two proteins mutated in autosomal-dominant hereditary spastic paraplegia, are binding partners. Hum. Mol. Genet. 15, 307–318.
Sannerud, R., Marie, M., Nizak, C., Dale, H.A., Pernet-Gallay, K., Perez, F., Goud, B., Saraste, J., 2006. Rab1 defines a novel pathway connecting the pre-Golgi intermediate compartment with the cell periphery. Mol. Biol. Cell. 17, 1514–1526.
Schuster, C.M., Davis, G.W., Fetter, R.D., Goodman, C.S., 1996. Genetic dissection of structural and functional components of synaptic plasticity. I. Fasciclin II controls synaptic stabilization and growth. Neuron 17, 641–654.
Sherwood, N.T., Sun, Q., Xue, M., Zhang, B., Zinn, K., 2004. *Drosophila* spastin regulates synaptic microtubule networks and is required for normal motor function. PLoS Biol. 2, e429.
Snapp, E.L., Iida, T., Frescas, D., Lippincott-Schwartz, J., Lilly, M.A., 2004. The fusome mediates intercellular endoplasmic reticulum connectivity in *Drosophila* ovarian cysts. Mol. Biol. Cell. 15, 4512–4521.
Soderblom, C., Blackstone, C., 2006. Traffic accidents: molecular genetic insights into the pathogenesis of the hereditary spastic paraplegias. Pharmacol. Ther. 109, 42–56.
Stewart, B.A., Atwood, H.L., Renger, J.J., Wang, J., Wu, C.F., 1994. Improved stability of *Drosophila* larval neuromuscular preparations in haemolymph-like physiological solutions. J. Comp. Physiol. [A] 175, 179–191.
Torroja, L., Packard, M., Gorczyca, M., White, K., Budnik, V., 1999. The *Drosophila* beta-amyloid precursor protein homolog promotes synapse differentiation at the neuromuscular junction. J. Neurosci. 19, 7793–7803.
Trotta, N., Orso, G., Rossetto, M.G., Daga, A., Broadie, K., 2004. The hereditary spastic paraplegia gene, spastin, regulates microtubule stability to modulate synaptic structure and function. Curr. Biol. 14, 1135–1147.
Waterman-Storer, C.M., Salmon, E.D., 1998. Endoplasmic reticulum membrane tubules are distributed by microtubules in living cells using three distinct mechanisms. Curr. Biol. 8, 798–806.
Wood, J.D., Landers, J.A., Bingley, M., McDermott, C.J., Thomas-McArthur, V., Gleadall, L.J., Shaw, P.J., Cunliffe, V.T., 2006. The microtubule-severing protein Spastin is essential for axon outgrowth in the zebrafish embryo. Hum. Mol. Genet. 15, 2763–2771.
Zhao, X., Alvarado, D., Rainier, S., Lemons, R., Hedera, P., Weber, C.H., Tukel, T., Apak, M., Heiman-Patterson, T., Ming, L., Bui, M., Fink, J.K., 2001. Mutations in a newly identified GTPase gene cause autosomal dominant hereditary spastic paraplegia. Nat. Genet. 29, 326–331.
Zhu, P.P., Patterson, A., Lavoie, B., Stadler, J., Shoeb, M., Patel, R., Blackstone, C., 2003. Cellular localization, oligomerization, and membrane association of the hereditary spastic paraplegia 3A (SPG3A) protein atlastin. J. Biol. Chem. 278, 49063–49071.
Zhu, P.P., Soderblom, C., Tao-Cheng, J.H., Stadler, J., Blackstone, C., 2006. SPG3A protein atlastin-1 is enriched in growth cones and promotes axon elongation during neuronal development. Hum. Mol. Genet. 15, 1343–1353.
Zito, K., Parnas, D., Fetter, R.D., Isacoff, E.Y., Goodman, C.S., 1999. Watching a synapse grow: noninvasive confocal imaging of synaptic growth in *Drosophila*. Neuron 22, 719–729.